Chemistry of Sulfur Oxides on Transition Metals. II. Thermodynamics of Sulfur Oxides on Platinum(111)

Xi Lin

Department of Chemistry, Massachusetts Institute of Technology, Cambridge, Massachusetts 02139-4301

William F. Schneider

Physical and Environmental Sciences Department, Ford Motor Company, MD 3083-SRL, Dearborn, Michigan 48121-2053

Bernhardt L. Trout*

Department of Chemical Engineering, Massachusetts Institute of Technology, Cambridge, Massachusetts 02139-4301

Received: May 12, 2003; In Final Form: September 5, 2003

The thermodynamics of S, O, SO, SO_2, SO_3, and SO_4 chemisorption on the Pt(111) surface are studied using first-principles density functional theory (DFT) computations. The adiabatic potential energy surfaces of SO_x ($x = 1$, 2, 3, and 4) on Pt(111) are probed systematically to yield comprehensive sets of local minima. The most energetically stable surface species are found to include always a tetrahedral S center bound to x O atoms and $4 - x$ surface Pt atoms. Novel surface reconstructions are observed at the highest coverages and sulfur oxidation states. Calculated vibrational spectra are used to assign observed surface spectra. The SO_x adsorbates experience strong lateral repulsion due to dipole−dipole interactions, and a procedure is developed to extrapolate these effects to low coverage. At low coverage, all SO_x adsorbates are found to be energetically unstable with respect to dissociation to atoms. Molecular SO_x moieties on the Pt(111) surface thus owe their existence to a combination of kinetic barriers to dissociation and lateral interaction effects. At high coverage or in an oxygen-saturated background, SO_4 becomes the preferred SO_x species on Pt(111), consistent with observation.

I. Introduction

The chemistry of sulfur-containing molecules on transition metal catalysts has been of interest to scientists for more than 2 decades.[1−3] It has consequences for the poisoning of these catalysts under both oxidizing and reducing conditions. However, sulfur chemistry on transition metal surfaces is so complicated that it remains far from being well understood. Major difficulties in experiments are in part due to the existence of various coadsorbed surface sulfur species, even when pure sulfur oxides, such as SO_2, are introduced from the gas phase to single crystal surfaces. Moreover, there has been very little work performed on evaluating the energetics or thermodynamics of adsorption of sulfur oxides or reactions of them. In fact, the only energetic number of sulfur oxides on Pt that we are aware of is a binding energy of SO_2 on Pt(111) of 100−150 kJ/mol from temperature-programmed desorption (TPD) experiments.[4] Having some energetic data or, moreover, having substantial data on the thermodynamics of adsorption and interconversion of sulfur oxide species would be a tremendous aid in better understanding these catalytic systems. The latter is a major accomplishment in the work presented here.

There are also uncertainties in the identification of vibrational spectra in surface science experiments. From standard surface experiments, such as high resolution electron energy loss spectroscopy (HREELS) and near-edge X-ray absorption fine structure (NEXAFS), molecularly chemisorbed SO_2 is detected on Pt(111) at temperatures below 130 K.[2,5−7] However, Sun et al. were unable to assign two new vibrational features in their HREELS experiments that appeared as the temperature was raised to 190 K,[6] in large part because only the vibrational frequencies of the gas-phase sulfur oxides and a limited number of sulfur oxides on other metal surfaces were available as guides. Further confusion comes from an independent HREELS experiment performed by Wilson et al., who did not detect either of these two new vibrational features at the same temperature.[8] In contrast, Wilson et al.[8] obtained several new vibrational features by pretreating the Pt(111) surface with the gas-phase oxygen, although the assignment of these three HREELS features was obscure.[8]

In this article, we present a comprehensive set of thermodynamic data for the adsorption of sulfur oxides and related species, including S, O, SO, SO_2, SO_3, and SO_4, on Pt(111) based on first-principles density functional theory (DFT) computations, and including the effects of surface coverage. In addition, we clarify the experimental observations by identifying vibrational modes of stable surface species and individual important elementary reactions on the Pt(111) single-crystal surface at low and intermediate temperatures. The important consequences of coverage and therein intermolecular interactions on stable surface species and surface reactions are emphasized. By obtaining a fundamental understanding of surface sulfur

* To whom all correspondence should be addressed. E-mail: trout@mit.edu.

10.1021/jp035306h CCC: $27.50
Published on Web 12/02/2003

chemistry, we aim to provide insight into chemical reactivity as a step toward the design of sulfur resistant transition metal catalysts.

II. Computational Details

The GNU publicly licensed software DACAPO[9] was used for all computations in this study. A three-layer slab model was used for the main calculations, and the convergence in binding structures and energies of this three-layer model was evaluated by comparison to calculations performed on a four-layer model. The atoms of the bottom layer were fixed at calculated bulk positions (given by the lattice constant $a = 4.00$ Å). A vacuum of ~10 Å was used to separate the slabs, and one additional external dipole layer was generated self-consistently in the middle of the vacuum to cancel the dipole interactions between slabs. The core electrons of all the atoms were treated using ultrasoft pseudopotentials[10,11] with an energy cutoff of 25 Ry for both electronic wave function and density. The *d*-channel was included explicitly to ensure a more accurate treatment of the sulfur core.[12] The PW91[13] gradient corrected exchange-correlation functional was used in the self-consistent DFT calculations. A 0.2 eV electronic temperature was introduced to sample the bands in the reciprocal space, and the energy was extrapolated to 0 K. The finite temperature smearing allowed efficient convergence in band energy computations even with relatively coarse grid of *k*-points. In test calculations, decreasing the temperature broadening parameter to 0.1 eV[15,16] produced changes in adsorption energies <5 kJ/mol. Spin polarization effects were not considered to be important for the surface species and therefore were not modeled in the study except for the gas-phase species. Additional details of our computational techniques have been described in one of our previous papers.[14]

We performed some tests in order to evaluate the convergence of the calculations with respect to slab thickness and choice of temperature broadening parameter. Specifically, we computed the binding energies of SO_2 fcc η^2-S_b,O_a on Pt(111), SO_2 fcc η^3-S_a,O_a,O_a on Pt(111), and SO_2 fcc η^2-S_b,O_a on O-preadsorbed Pt(111) using both three- and four-layer slab models.[14] (See below for details on the adsorption configuration nomenclature.) The energies of adsorption for those three calculations for three vs four layers respectively in kJ/mol are as follows: 98 vs 90, 89 vs 80, and 11 vs 14, respectively. The slab thickness is seen to only qualitatively modify the adsorption energy; the effect on adsorbate geometry is even more minor, with deviations less than 0.01 Å. A recent study of O adsorption on Pt(111) reported negligible differences between four- and six-layer slabs.[17] These small changes are consistent with the relatively small relaxations of surface Pt (<0.15 Å) accompanying adsorption. In cases of more significant surface reconstruction (section III.C), thicker slabs would be essential to compute energies of adsorption accurately.

After determining the most energetically stable configurations for all of the sulfur oxide species, small independent displacements (~0.01 Å) along the Cartesian coordinates from the equilibrium positions of the adsorbate atoms were performed, and the finite differences of the resulting forces were taken to compute the Hessian matrices. The influence of the motion of the substrate metal atoms on the vibrational modes of the adsorbates was found to be negligible (refer to section III.D for detail), so for most of the vibrational frequency calculations, finite differences were performed on only the adsorbates. No symmetry was assumed a priori. The vibrational modes were obtained using the canonical transformations of phonons,[18] namely by diagonalizing the mass-weighted Hessian matrices obtained from the finite differences of *k*-point weighted forces. The equilibrium geometry at $^1/_4$ monolayer (ML) coverage was used as the reference point in our harmonic oscillator frequency calculations, where 1 ML is defined here as one adsorbate molecule per surface metal atom. Equality in the symmetric elements of the Hessian matrices was found, indicating that the finite difference computation was sufficiently accurate for the vibrational frequency determination. The ideal gas, rigid rotor, and harmonic oscillator approximations were used to calculate thermodynamic functions, such as the Gibbs free energies.[19] The adsorbates are assumed to be perfectly ordered at all coverages, so that configurational entropy is ignored.

III. Results and Discussion

A. Configurations and Energetics. Our computed ground states of gas-phase sulfur oxides and related gas-phase molecules are summarized as follows: O_2 is a triplet with an O−O bond length of 1.24 Å; atomic *S* is a triplet; SO is a triplet with an S−O bond length of 1.52 Å; SO_2 is a C_{2v} singlet with an S−O bond length of 1.47 Å; SO_3 is a D_{3h} singlet with an S−O bond length of 1.46 Å. More information has been reported in our previous papers.[3,12,14]

It has been shown both experimentally and computationally that chemisorbed atomic oxygen prefers fcc sites at $^1/_4$ ML coverage on the Pt(111) surface.[12,20] The calculated O binding energy is 411 kJ/mol. Coverages higher than $^1/_4$ ML are not considered here, because they do not form from O_2 and SO_2, except in the presence of special surface oxidizing agents, such as NO_2.[21]

Similar to chemisorbed atomic oxygen, chemisorbed atomic sulfur prefers fcc sites at $^1/_4$ ML coverage.[12] The calculated binding energy is 460 kJ/mol. Higher coverages have been reported from experiments,[22] and computational studies have shown that S switches to atop sites at coverages higher than $^1/_3$ ML.[23] The preference of atop sites at sulfur coverages beyond $^1/_3$ ML is expected, because at such high coverages sulfur atoms at fcc 3-fold sites have to share the surface Pt atoms, leading to significant decreases in the bonding energy.[14]

Like chemisorbed atomic sulfur, molecular SO prefers fcc sites, with the sulfur atom directly attached to the 3-fold sites on the metal surface. The binding configuration is named SO fcc η^1-S_f(O_f) in our nomenclature and is sketched in Figure 1a. Here fcc indicates that the adsorbed SO molecule sits primarily above an fcc site on the Pt(111) surface. Other possible cases include atop, bridge, and hcp, indicating that the adsorbate molecule locates primarily above an atop site, a bridge site, or an hcp site on the Pt(111) surface, respectively. η^n indicates that there are *n* atoms of the adsorbate molecule directly bound to the surface. Following the dash are the names of the atoms directly attached to the surface. Subscripts indicate the binding site of the atoms, where a, b, f, and h stand for atop, bridge, fcc, and hcp sites, respectively. If necessary, indirectly bound atoms might be marked in parentheses to show the special orientation of the adsorbate molecule. This nomenclature is also used in one of our previous studies.[14]

As shown in Table 1, the chemisorption energy of SO fcc η^1-S_f(O_f) is 259 kJ/mol at $^1/_4$ ML coverage. The Pt−S bond length is 2.27 Å (refer to Table 2), which is slightly shorter than the Pt−S bond for the chemisorbed atomic sulfur (2.29 Å) at the same coverage. The S−O bond length is 1.49 Å, which is also shorter than the gas-phase molecular S−O bond length of 1.52 Å. It is normally expected for adsorbed molecules to have longer internal bond lengths upon chemisorption to metal surfaces, because strong chemical bonding of chemisorbed

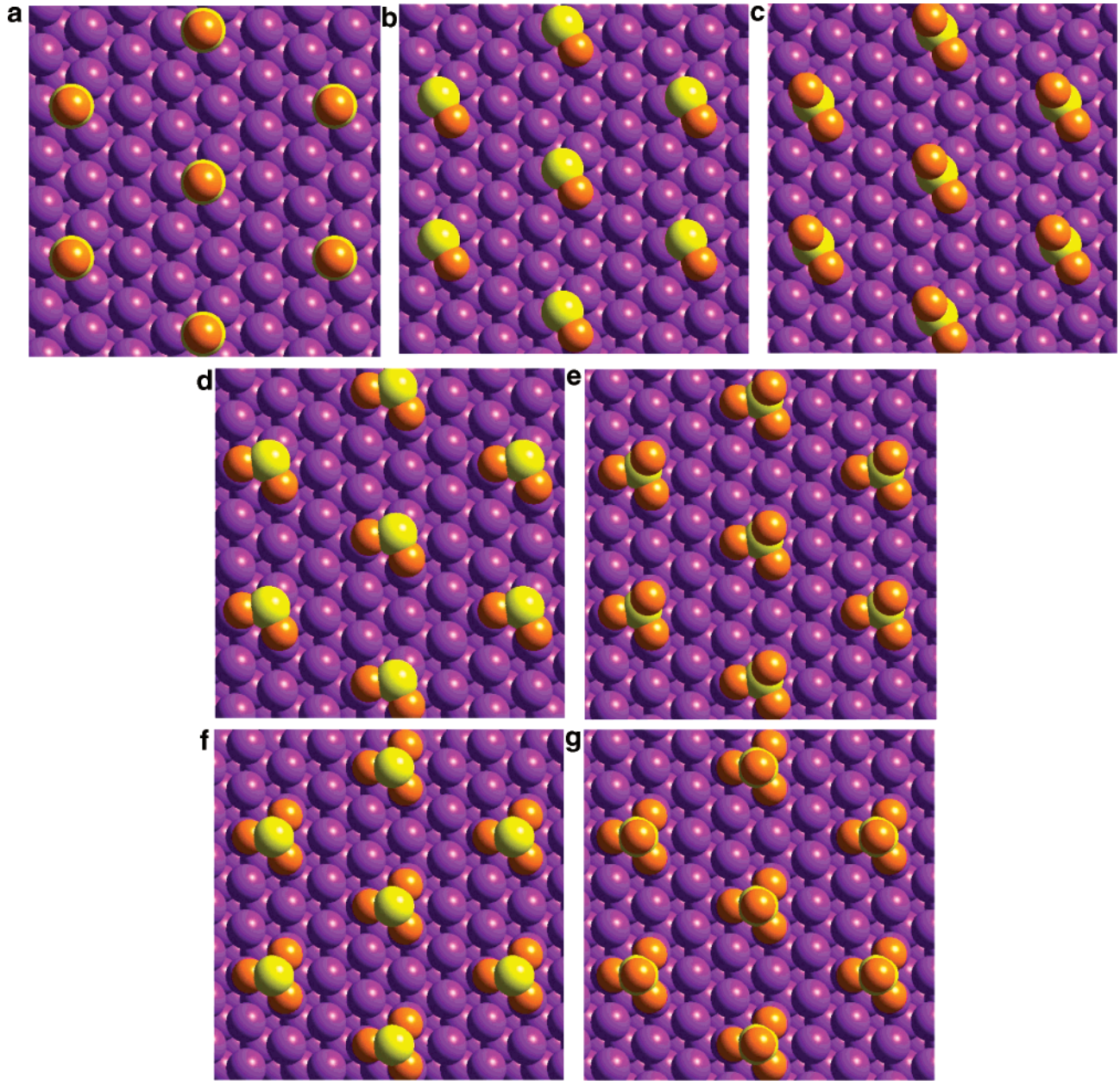

Figure 1. Molecular structures of strong binding configurations of SO_x ($x = 1$, 2, 3, and 4) at $^1/_9$ ML coverage on Pt(111): (a) SO fcc η^1-$S_f(O_f)$; (b) SO fcc η^2-S_b,O_a; (c) SO_2 fcc η^2-S_b,O_a; (d) SO_2 fcc η^3-S_a,O_a,O_a; (e) SO_3 fcc η^3-S_a,O_a,O_a; (f) SO_3 fcc η^3-O_a,O_a,O_a; (g) SO_4 fcc η^3-O_a,O_a,O_a. Note that the violet, orange, and yellow balls represent the Pt, O, and S atoms, respectively.

molecules to the metal atoms tends to decrease the internal bond strengths of the molecules, thus leading to longer internal bond lengths.[14] We do note that for other (metastable) configurations of bound SO, η^2-S_b,O_a in particular, we do observe an increase in bond length upon adsorption (Table 2). This is consistent with theoretical work published in the literature on adsorption of SO_x on Cu surfaces.[24] The strengthening of the S−O bond of SO fcc η^1-$S_f(O_f)$ upon chemisorption is further confirmed by an increase in the S−O stretching frequency from 1106 (gas phase) to 1169 cm^{-1} (adsorbed, uncorrected). (Refer to section III.D for details.) SO atop η^1-$S_a(O_a)$ and SO bridge η^1-$S_b(O_b)$ both are unstable with respect to SO fcc η^1-$S_f(O_f)$ and relax to this more stable configuration during geometry optimizations.

Several other SO configurations are close in energy to SO fcc η^1-$S_f(O_f)$. One of these is the sideways-bound SO fcc η^2-S_b,O_a (refer to Figure 1b and Tables 1 and 2), which is related to the most stable binding configuration of SO_2 by removal of the nonsurface-bound O. (Compare Figure 1b to Figure 1c.) A variation on SO fcc η^2-S_b,O_a, with only one surface-bound atom, is SO fcc η^1-$S_b(O_a)$, which is similarly related to the adsorbate configuration of SO_2 bridge η^1-S ⊥, where bridge indicates that the chemisorbed SO_2 sites primarily over a bridge site and ⊥ indicates that the SO_2 molecular plane is perpendicular to the line connecting the two bridge Pt atoms.[14]

Molecular SO binding at hcp 3-fold sites is similar to that of fcc 3-fold sites, with typical decreases in binding energies of less than 15 kJ/mol, typical decreases in internal S−O bond lengths of 0.02 Å or less, and typical increases in Pt−S and Pt−O bond lengths of 0.06 Å or less. The huge decrease in binding energy (∼300 kJ/mol) from SO fcc η^1-$S_f(O_f)$ to SO fcc η^1-$O_f(S_f)$ shows the importance of having the metal−sulfur bonds. A similar conclusion has been drawn from a previous study of SO_2 adsorption.[14] The negative binding energies of the metastable surface species in Table 1 are a consequence of strong, unfavorable lateral interactions at $^1/_4$ ML coverage, and these negative binding energies become positive when the

TABLE 1: Stable and Metastable Binding Configurations of SO, SO_3, and SO_4 on Pt(111): Binding Energies and *Z*-Axis Dipole Moments Perpendicular to the Metal Surface[a]

configurations	figure index	perpendicular dipole (D) p(2×2)	perpendicular dipole (D) p(3×3)	binding energy (kJ/mol) p(2×2)	binding energy (kJ/mol) p(3×3)
SO fcc η^1-$S_f(O_f)$	1a	−0.48	−0.75	258.82	284.70
SO fcc η^2-S_b,O_a	1b	0.21	0.16	249.92	267.90
SO hcp η^2-S_b,O_a		0.19		243.81	
SO hcp η^1-$S_h(O_h)$		−0.40		242.40	
SO hcp η^1-$S_b(O_a)$		−0.24		239.93	
SO fcc η^1-$S_b(O_a)$		−0.23		238.31	
SO bridge η^1-$O_b(S_b)$		1.27		−24.21	
SO fcc η^1-$O_f(S_f)$		1.25		−28.86	
SO hcp η^1-$O_h(S_h)$		1.43		−35.03	
SO_3 fcc η^3-S_a,O_a,O_a	1e	−1.13	−1.76	113.24	138.40
SO_3 hcp η^3-S_a,O_a,O_a		−1.13		110.12	
SO_3 fcc η^3-O_a,O_a,O_a	1f	−0.19	−0.52	98.00	127.34
SO_3 hcp η^3-O_a,O_a,O_a		−0.19		96.00	
SO_3 atop η^4-S_a,O_b,O_b,O_b		−1.42		46.43	
SO_3 atop η^4-S_a,O_h,O_h,O_h		−1.36		39.29	
SO_3 atop η^4-S_a,O_f,O_f,O_f		−1.37		38.77	
SO_3 fcc η^4-S_f,O_a,O_a,O_a		0.38		16.45	
SO_3 hcp η^4-S_h,O_a,O_a,O_a		0.20		13.90	
SO_3 hcp η^4-S_h,O_f,O_f,O_f		0.21		13.35	
SO_3 fcc η^4-S_f,O_h,O_h,O_h		0.22		12.97	
SO_4 fcc η^3-O_a,O_a,O_a	1g	−1.67	0.15	298.38	341.42
SO_4 hcp η^3-O_a,O_a,O_a	1h	−1.66		297.60	
SO_4 fcc η^1-$O_f(SO_3)_f$		−0.71		184.82	
SO_4 atop η^4-S_a,O_h,O_h,O_h		−1.97		89.21	

[a] The direction of the *Z*-axis dipole moments is chosen from the substrate to the adsorbate, where the convention of dipole moments pointing from negative charges to positive charges is used. The binding energies of all species are computed with respect to the most stable gas-phase species and the clean Pt(111) surface, while the binding energies of SO_4 are computed with respect to a reference of gas-phase SO_2 and O_2.

coverage is decreased.[14] SO atop η^1-$O_a(S_a)$ is unstable and becomes SO hcp η^2-S_b,O_a during the geometry relaxation. SO bridge η^1-$O_b(S_b)$ is metastable, but the O−S bond is not perpendicular to the metal surface, forming an angle of 68°. All of the configurations having directly bound oxygen and indirectly bound sulfur exhibit large perpendicular dipole moments pointing away from the surface.

As discussed previously,[14] 20 metastable configurations have been identified for chemisorbed molecular SO_2 on Pt(111), among which there are two distinct strongly bound types with binding energies of ∼100 kJ/mol at $^1/_4$ ML. One has the SO_2 molecular plane perpendicular to the metal surface (for example, SO_2 fcc η^2-S_b,O_a of Figure 1c), and the other has the molecular plane parallel to the metal surface (for example, SO_2 fcc η^3-S_a,O_a,O_a of Figure 1d). Other theoretical studies have found SO_2 adsorbed in a 3-fold coordination on various metal and metal oxide surfaces.[24,25]

The most energetically favored configuration of SO_3, namely SO_3 fcc η^3-S_a,O_a,O_a, is related to the flat-lying SO_2 fcc η^3-S_a,O_a,O_a (compare Figure 1d with Figure 1e.) Unlike planar, gas-phase SO_3, the S center in SO_3 fcc η^3-S_a,O_a,O_a is approximately tetrahedrally bound to three O and one surface Pt atom. Tables 1 and 2 include four weakly bound planar SO_3 configurations, namely SO_3 fcc η^4-S_f,O_a,O_a,O_a, SO_3 hcp η^4-S_h,O_a,O_a,O_a, SO_3 hcp η^4-S_h,O_f,O_f,O_f, and SO_3 fcc η^4-$S_f,$-O_h,O_h,O_h, but each of these metastable configurations has only 10% to 15% of the binding energy of the tetrahedral SO_3 fcc η^3-S_a,O_a,O_a at $^1/_4$ ML coverage. As shown in Table 2, the dihedral angle is 31° between the plane formed by the three surface-bound atoms (namely, one sulfur atom and two oxygen atoms) and the plane formed by the three oxygen atoms. The O−S−O angle in the plane formed by the three surface-bound atoms is 107°, which is almost identical to the same angle in SO_2 fcc η^3-S_a,O_a,O_a, 106°.[14] Further comparisons of these two configurations show very close matches in both S−O (1.56 vs 1.55 Å) and Pt−S (2.31 vs 2.33 Å) bond lengths, and a slightly larger deviation in the Pt−O bond lengths (2.16 vs 2.23 Å). Therefore, we conclude that the surface bonding of SO_3 fcc η^3-S_a,O_a,O_a is closely related to that of SO_2 fcc η^3-S_a,O_a,O_a, the latter of which has been discussed in detail previously.[14] In SO_3 fcc η^3-S_a,O_a,O_a, the O−S−O bond angles involving the O atom not bound to the surface are larger than the O−S−O angle of the three directly bound atoms (113 vs 107°), the difference being due to the geometric constraints imposed by coordination to the surface metal atoms. The S−O bond with the nonsurface bound O is 1.46 Å, which is the same as that of the S−O bond of the gas-phase SO_3.

Another type of strongly bound configuration of chemisorbed SO_3 involves three directly bound O atoms, e.g., SO_3 fcc η^3-O_a,O_a,O_a (Figure 1f). A similar structure involving three directly bound oxygen atoms (C_{3v} symmetry) has been reported on Cu(111) in a chemical-shift, normal incidence X-ray standing waves study (CS−NIXSW) combined with NEXAFS by Jackson et al.[26] Because all three oxygen atoms are bound to the metal surfaces, the three S−O bonds become fairly stretched on the surface (1.57 Å) compared to the gas-phase (1.46 Å). However, the Pt−O bonds are shorter than those in any other chemisorbed SO_3 configuration that has been found in our study. Similar to the experimental observation by Jackson et al.,[26] the sulfur atom no longer shares the same plane as the three oxygen atoms, and the out-of-plane dihedral angle of the sulfur atom is about 39°, which is the largest out-of-plane dihedral angle among all chemisorbed SO_3 configurations. The binding energy of SO_3 fcc/hcp η^3-O_a,O_a,O_a is ∼15 kJ/mol less than that of SO_3 fcc/hcp η^3-S_a,O_a,O_a.

Because of the relative height of the S atom above the metal surface compared to the O atoms, the dipole moment normal to the Pt(111) plane in fcc/hcp η^3-O_a,O_a,O_a is much smaller than that in fcc/hcp η^3-S_a,O_a,O_a (−0.19 vs −1.13 D, where the negative sign indicates a dipole pointing from the adsorbate to the metal surface). Even larger dipoles (−1.36 to −1.42 D) are observed in three configurations having sulfur over atop sites. These metastable configurations have a third to half of the binding energies of the most strongly bound configurations. Very weakly bound configurations, with binding energies ranging from 13 to 16 kJ/mol, are rather planar. Both the S−O bonds and the O−S−O angles in these configurations are identical to the values of gas-phase SO_3, while all the sulfur and oxygen atoms are at least 3 Å away from the surface metal atoms. No configurations of chemisorbed SO_3 have been identified with bi-coordinated sulfur atoms.

There is a similar structural connection between chemisorbed η^3-O_a,O_a,O_a SO_3 and SO_4. Comparisons of these two configurations at the same 3-fold sites indicate very close matches in geometric parameters, including S−O (1.57 vs 1.55 Å) and Pt−O (2.14 vs 2.12 Å) bonds, O−S−O angles (107 vs 108°), and the dihedral angles between the S−O−O planes and the O−O−O plane (39 vs 38°). (Refer to Figure 1, parts f and g.) Tetrahedral SO_4 has fewer orientational binding possibilities that do SO, SO_2, and SO_3.[14] The SO_4 fcc η^1-$O_f(SO_3)_f$ configuration is an interesting outlier which is best described as SO_3 weakly bound (by 17 kJ/mol) to an O-covered Pt(111) surface. The SO_3 fragment is identical in structure to gas-phase SO_3 and sits 2.79 Å above a surface O. The last metastable configuration in

TABLE 2: Binding Geometry of Pt(111)−p(2×2)−SO_x (x = 1, 3, and 4)[a]

	bond length (Å)			bond angles (deg)	
configurations	S−O	Pt−O	Pt−S	SO orientation or O−S−O angle	dihedral between S−O−O and O−O−O planes
SO fcc η^1-$S_f(O_f)$	1.49		2.27 (×3)	⊥	
SO fcc η^2-S_b,O_a	1.58	2.22	2.30 (×2)	∥	
SO hcp η^2-S_b,O_a	1.57	2.28	2.31 (×2)	∥	
SO hcp η^1-$S_h(O_h)$	1.49		2.29 (×3)	⊥	
SO hcp η^1-$S_b(O_a)$	1.51		2.32 (×2)	32	
SO fcc η^1-$S_b(O_a)$	1.51		2.32 (×2)	32	
SO bridge η^1-$O_b(S_b)$	1.58		2.39 (×2)	68	
SO fcc η^1-$O_f(S_f)$	1.59	2.45 (×3)		⊥	
SO hcp η^1-$O_h(S_h)$	1.58	2.50 (×3)		⊥	
SO_3 fcc η^3-S_a,O_a,O_a	1.46	2.16 (×2)	2.31	107	31
	1.56 (×2)			113 (×2)	35 (×2)
SO_3 hcp η^3-S_a,O_a,O_a	1.46	2.18 (×2)	2.31	108	31
	1.56 (×2)			112 (×2)	34 (×2)
SO_3 fcc η^3-O_a,O_a,O_a	1.57 (×3)	2.14 (×3)		107 (×3)	39 (×3)
SO_3 hcp η^3-O_a,O_a,O_a	1.57 (×3)	2.14 (×3)		107 (×3)	39 (×3)
SO_3 atop η^4-S_a,O_b,O_b,O_b	1.49 (×3)	3.00 (×3)	2.36	117 (×3)	21 (×3)
		3.02 (×3)			
SO_3 atop η^4-S_a,O_h,O_h,O_h	1.49 (×3)	3.02 (×3)	2.38	117 (×3)	20 (×3)
		3.20 (×6)			
SO_3 atop η^4-S_a,O_f,O_f,O_f	1.49 (×3)	3.02 (×3)	2.38	117 (×3)	20 (×3)
		3.22 (×6)			
SO_3 fcc η^4-S_f,O_a,O_a,O_a	1.46 (×3)	3.21 (×3)	3.56 (×3)	120 (×3)	2 (×3)
SO_3 hcp η^4-S_h,O_a,O_a,O_a	1.46 (×3)	3.13 (×3)	3.50 (×3)	120 (×3)	2 (×3)
SO_3 hcp η^4-S_h,O_f,O_f,O_f	1.46 (×3)	3.60 (×6)	3.61 (×3)	120 (×3)	2 (×3)
		3.69 (×3)			
SO_3 fcc η^4-S_f,O_h,O_h,O_h	1.46 (×3)	3.74 (×3)	3.74 (×3)	120 (×3)	2 (×3)
		3.82 (×3)			
SO_4 fcc η^3-O_a,O_a,O_a	1.45	2.12 (×3)		108 (×3)	33 (×3)
	1.55 (×3)			110 (×3)	36 (×3)
					38 (×3)
SO_4 hcp η^3-O_a,O_a,O_a	1.45	2.12 (×3)		108 (×3)	33 (×3)
	1.55 (×3)			111 (×3)	36 (×3)
					37 (×3)
SO_4 fcc η^1-$O_f(SO_3)_f$	2.79	2.08 (×3)		120 (×3)	1 (×3)
	1.46 (×3)				
SO_4 atop η^4-S_a,O_h,O_h,O_h	1.46	2.70 (×3)	2.85	107 (×3)	32 (×3)
	1.55 (×3)	2.70 (×6)		112 (×3)	35 (×3)
					38 (×3)

[a] The number of bonds of identical lengths due to the underlying symmetry is indicated in parentheses. Note that in our calculation the reference molecules SO (triplet), SO_2 (C_{2v}), and SO_3 (D_{3h}) have S−O bond lengths of 1.52, 1.47, and 1.46 Å, respectively.

Tables 1 and 2 is the chemisorbed SO_4 atop η^4-S_a,O_h,O_h,O_h, which has a binding energy only ∼30% of the most strongly bound configuration, SO_4 fcc η^3-O_a,O_a,O_a. Two relatives of the SO_4 atop η^4-S_a,O_h,O_h,O_h configuration produce unexpected surface reconstructions discussed in section III.C: SO_4 atop η^4-S_a,O_b,O_b,O_b reconstructs to $(SO_4)_{sr}$ η^3-O_a,O_a,O_a, and SO_4 atop η^4-S_a,O_f,O_f,O_f reconstructs to $(SO_4)_{sr}$ η^3-O_b,O_b,O_b, where the subscript sr means surface reconstructed.

In summary, SO_x chemisorption on Pt(111) evidences a rich variety of binding configurations. Two general observations emerge about the most stable sulfur oxide configuration. First, the S center prefers to be tetrahedrally coordinated. Specifically, the S atom of SO_4 fcc η^3-O_a,O_a,O_a is surrounded by four O atoms, the S atom of SO_3 fcc η^3-S_a,O_a,O_a bonds atop one surface Pt atom in addition to three O atoms, the S atom of SO_2 fcc η^2-S_b,O_a bridges two surface Pt atoms to complement its two O atoms, and the S atom of SO fcc η^1-$S_f(O_f)$ occupies a 3-fold fcc hollow site on the Pt(111) surface. Second, the most stable configurations are connected by common structures, i.e., η^1-S_f links S to SO, η^2-S_b,O_a links SO to SO_2, η^3-S_a,O_a,O_a links SO_2 to SO_3, and η^3-O_a,O_a,O_a links SO_3 to SO_4.

B. Dipole Rule for Coverage Effect. The nonvanishing dipoles produced by highly electronegative adsorbates like the sulfur oxides yields long-range lateral interactions. In a previous study, we have shown that the binding energy of SO_2 can be extrapolated to the zero-coverage limit by taking advantage of the fact that the interactions are dipole−dipole in form.[14] In this paper, we apply this rule to chemisorbed O, S, SO, SO_3, and SO_4 to estimate binding energies at zero coverage. The basic idea is that when the coverage is lower than some threshold value such that direct chemical bonding interactions among the adsorbates are small, the nonvanishing dipole−dipole repulsive interactions dominate the lateral interactions for any given neutral surface system. Therefore, the binding energy should scale as $1/r^3$, where r is the physical separation of the two nearest dipoles. The results are listed in Table 3 and plotted in Figure 2. As shown in Table 1 and previously,[14] the strong lateral dipole interactions influence the absolute binding energies, but not the binding geometries and relative orderings in binding energies among different configurations. Important applications of this dipole rule include the energy analysis and the non-Langmuirian isotherms, presented in section III, parts E−H.

C. Surface Reconstruction. In general, close-packed surfaces are regarded to be less prone to reconstruction upon chemisorption of gas-phase molecules. Experimentally, surface reconstruction of Cu(111) caused by sulfur-containing molecules such as SO_2,[27] SO_4,[28] and atomic S[29] has been reported. To our knowledge, no surface reconstruction has been observed either experimentally or computationally on the Pt(111) surface by sulfur-containing molecules.

TABLE 3: Coverage Dependence of Binding Energy Due to the Lateral Interaction of Sulfur Oxides on Pt(111) from 1/4 ML to the Zero Coverage Limit[a]

	binding energy (kJ/mol)					
	p(2×2) or 1/4 ML	$(\sqrt{7}\times\sqrt{7})$ R19° or 1/7 ML	*p*(3×3) or 1/9 ML	$(\sqrt{13}\times\sqrt{13})$ R14° or 1/13 ML	p(4×4) or 1/16 ML	0 ML (est)
O	411.05		426.36		426.37	429.87
S	460.34		491.93		493.27	500.11
SO	258.82	284.66	284.70	293.75	289.70	297.03
SO_2	97.68	116.15	117.57	126.12	126.79	129.62
SO_3	113.24	136.30	138.40	147.06	145.02	150.67
SO_4	298.38	338.19	341.42	347.98	345.83	356.51

[a] Note that the binding energies of SO_4 are computed with respect to a reference of gas-phase SO_2 and O_2.

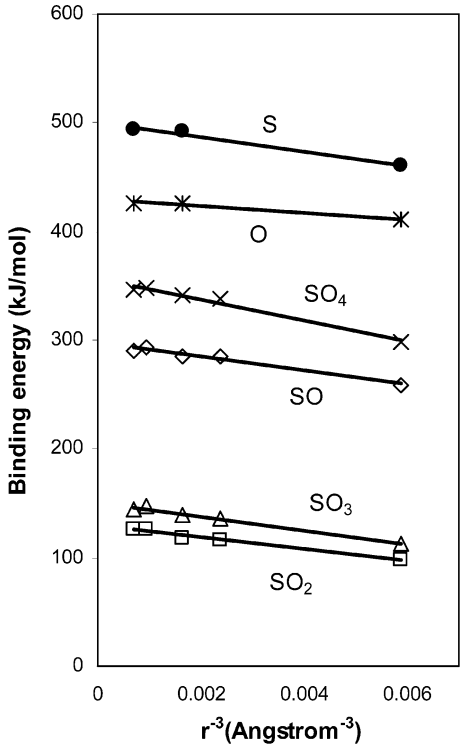

Figure 2. Correlation between the binding energies of O and SO_x (x = 0, 1, 2, 3, and 4) to Pt(111) and the shortest distance between two adsorbates to the −3 power. The intercepts on the y axis are the binding energies at the limit of infinite separation of adsorbates. The slopes give the estimates of the effective dipole moments. Refer to Table 3 for detail.

TABLE 4: Surface Reconstruction at One-fourth Coverage: Binding Energies and Perpendicular Dipole Moments[a]

configurations	figure index	*Z*-axis dipole (D)	binding energy (kJ/mol)
$(SO_4)_{sr}$ η^3-O_a,O_a,O_a	3a	−1.73	305.01
$(SO_4)_{sr}$ η^3-O_b,O_b,O_b	3b	−1.80	156.43
$(SO_3)_{sr}$ η^3-S_a,O_a,O_a	3c	−1.13	104.63
$(SO_3)_{sr}$ η^3-O_a,O_a,O_a	3d	−0.25	102.57
$(SO_2)_{sr}$ η^3-S_a,O_a,O_a	3e	−0.87	83.56

[a] Note that the binding energies of SO_4 are computed with respect to a reference of gas-phase SO_2 and O_2.

We observed two different surface-reconstructions accompanying adsorption of SO_4 at 1/4 ML, namely $(SO_4)_{sr}$ η^3-O_a,O_a,O_a and $(SO_4)_{sr}$ η^3-O_b,O_b,O_b. (Refer to Table 4 and Figure 3, parts a and b, for details.) Significantly, it is found that the binding energy of $(SO_4)_{sr}$ η^3-O_a,O_a,O_a (305 kJ/mol) is 7 kJ/mol larger than that of SO_4 fcc η^3-O_a,O_a,O_a (298 kJ/mol), which is the most stable configuration without surface reconstruction (refer to Table 1). The energetics indicates that the surface reconstruction should be spontaneous upon chemisorption of SO_4 at 1/4 ML coverage. From $(SO_4)_{sr}$ η^3-O_a,O_a,O_a, several surface-reconstructed SO_3 species—$(SO_3)_{sr}$ η^3-S_a,O_a,O_a and $(SO_3)_{sr}$ η^3-O_a,O_a,O_a—and SO_2 species—$(SO_2)_{sr}$ η^3-S_a,O_a,O_a—have been deduced. Refer to Table 4 and Figure 3, parts c−e for details. We note that all of these surface-reconstructed species have binding energies comparable to the corresponding strongly bound species without the surface reconstructions. As shown in Figure 3, parts a−e, these reconstructed metal surfaces still have hexagonal symmetry along the surface plane, partially due to the fixed p(2×2) supercell; however, they no longer have the ABC(ABC) layers along the (111) direction of fcc crystals, but rather layers of the type ABA(BAB). (Note that we did not impose symmetry on the atoms inside the supercell for any of our calculations, section II.) Further investigations on surface reconstruction depth and supercell relaxation would be needed for a full characterization. Since the binding of the SO_x species to the unreconstructed Pt(111) surface does not seem to be extremely sensitive to either additional metal layers or the hexagonal symmetry constraint on the supercell, we expect, however, that including more degrees of freedom for relaxation will make the reconstructed surface even more (or at least equally) stable compared to the unreconstructed surface. It is found that all of the surface reconstructions observed at 1/4 ML coverage disappear when the coverage is lowered to 1/9 ML. For example, $(SO_4)_{sr}$ η^3-O_a,O_a,O_a becomes SO_4 hcp η^3-O_a,O_a,O_a, and $(SO_3)_{sr}$ η^3-S_a,O_a,O_a becomes SO_3 hcp η^3-S_a,O_a,O_a.

D. Vibrational Mode Analyses. Comparisons of the computed frequencies with well-established experimental data are listed in Table 5 and plotted in Figure 4a. A downshift of ∼36 cm^{-1} with a scaling factor of 1.0 is observed in our calculated harmonic frequencies, and this correction is applied to all the computed frequencies listed in Table 6. It is shown in Figure 4b that only a minor, constant upshift in frequency occurs (leading to frequencies closer to the experimental data) when the first-row substrate metal atoms, in addition to the adsorbate atoms, are included explicitly in the harmonic oscillator calculation. Such a small change is expected since transition metal atoms such as Pt are heavier than S and O. Experimentally, it was shown that there were also only minor differences in harmonic frequencies (∼9 cm^{-1}) when the coverage of atomic oxygen was increased from 1/4 to 3/4 ML.[21] On the basis of the dipole rule analyses mentioned in the section III.C, we expect that even smaller deviations in the harmonic frequencies may occur from 1/4 ML to lower coverages, which allows us to safely apply the harmonic frequencies computed at the 1/4 ML to all other lower coverages.

As shown in Figure 4, parts c−e, and Table 6, the computed vibrational frequencies of strongly bound surface sulfur oxide species clearly fall into three bands. The low-frequency band has a broad range from 130 to 620 cm^{-1} and contains various vibrational motions involving all of the atoms in the adsorbates, such as frustrated translation, frustrated rotation, molecular

TABLE 5: Comparison of Calculated Vibrational Mode Frequencies (cm^{-1}) to Experimental Values[f]

Gas-phase SO	1106 1149[a] (stretching)					
Gas-phase SO_2	467 518[a] (bending)	1111 1151[a] (symmetric stretching)	1308 1362[a] (asymmetric stretching)			
Gas-phase SO_3	469 530[a] (asymmetric stretching)	473 498[a] (out-of-plane deforming)	475 530[a] (asymmetric stretching)	1012 1065[a] (symmetric stretching)	1330 1391[a] (asymmetric stretching)	1331 1391[a] (asymmetric stretching)
O fcc	352 400[b] (frustrated translation)	353 400[b] (frustrated translation)	466 480[b]/466[c] (stretching)			
SO_2 fcc η^2-S_b,O_a	488 540[d]/525[e] (bending)	913 940[d,e] (symmetric stretching)	1224 1252[d]/1245[e] (asymmetric stretching)			

[a] Constants of gas-phase molecules[36] [b] EELS[37] [c] HREELS [21] [d] HREELS[6] [e] HREELS[8] [f] The first row for each species presents our computed values, and the second row for each species presents experimental data. Multiple experimental entries are from different sources and separated by slashes. When further clarification on the computed normal modes is needed, arrows (with relative scaling length) and dots are used to represent the corresponding vibration directions (with relative scaling strength) and still atoms, respectively. The arrows and dots at the center represent the sulfur atoms, and the rest of the arrows and dots represent the oxygen atoms.

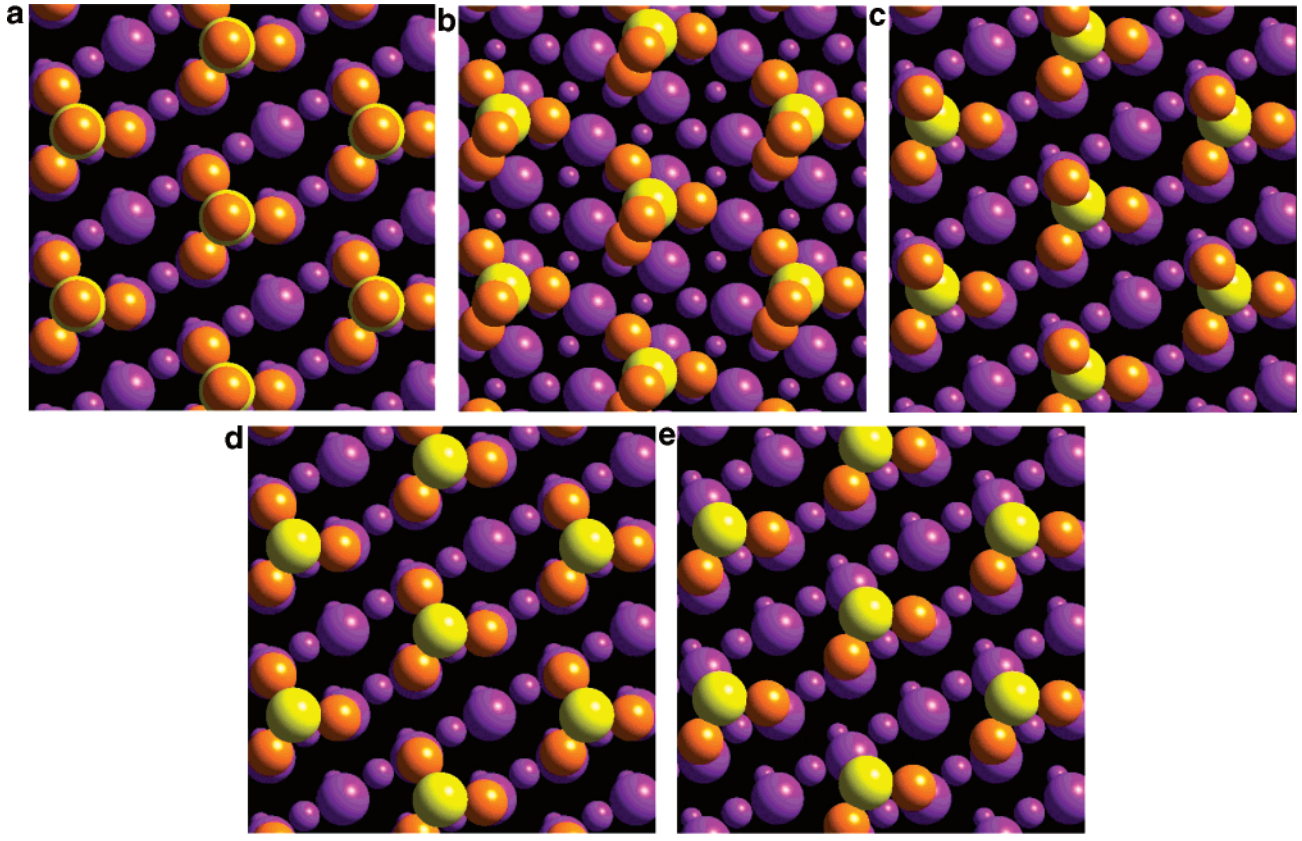

Figure 3. Surface reconstruction upon chemisorption of SO_x ($x = 2, 3, 4$) at $^1/_4$ ML surface coverage on Pt(111): (a) $(SO_4)_{sr}$ η^3-O_a,O_a,O_a; (b) $(SO_4)_{sr}$ η^3-O_b,O_b,O_b; (c) $(SO_3)_{sr}$ η^3-S_a,O_a,O_a; (d) $(SO_3)_{sr}$ η^3-O_a,O_a,O_a; (e) $(SO_2)_{sr}$ η^3-S_a,O_a,O_a. The violet, orange, and yellow balls represent the Pt, O, and S atoms, respectively. The large balls represent the adsorbate and the first layer Pt atoms, and the medium and small balls represent the second and third layers of the Pt atoms, respectively.

stretching, out-of-plane deforming, and bending. In contrast, the high-frequency band involves only pure S−O* stretching motions, with vibrational frequencies between 1200 and 1320 cm^{-1}, where O* represents the indirectly bound oxygen atom.

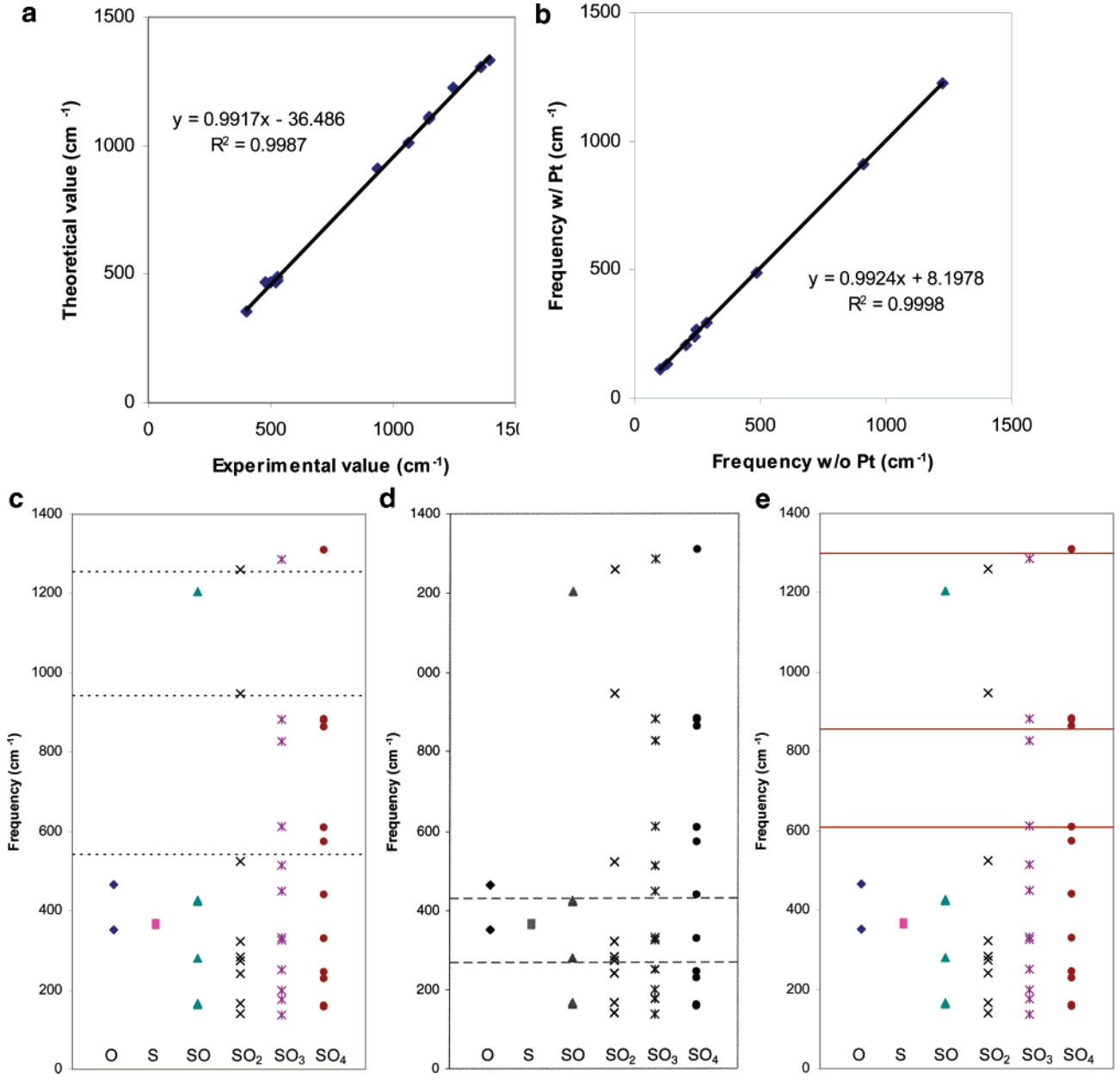

Figure 4. Vibrational frequency analyses. (a) Comparison of the theoretical vibrational frequencies to the well-documented experimental values of gas-phase SO_x ($x = 1$, 2, and 3), O fcc, and SO_2 fcc η^2-S_b,O_a. The solid line is the least-squares fit. Refer to Table 5 for detail. (b) Effect of explicitly including motions of the first-layer surface metal atoms on the computed vibrational frequencies of the SO_2 fcc η^2-S_b,O_a. The solid line is the least-squares fit. Refer to Table 6 for detail. (c) Identification of experimentally observed surface species by comparing vibrational frequencies experimentally observed at 130 K[6] (dotted lines) with calculated values of stable surface sulfur oxides and related surface species (data points). (d) Identification of experimentally observed surface species by comparing vibrational frequencies experimentally observed at 190 K[6] (dashed lines) with calculated values of stable surface sulfur oxides and related surface species (data points). (e) Identification of experimentally observed surface species by comparing vibrational frequencies experimentally observed on an oxygen precovered surface at 160 K[8] (solid lines) with calculated values of stable surface sulfur oxides and related surface species (data points).

The intermediate-frequency band, between 820 cm^{-1} to 1000 cm^{-1}, is also a narrow band that consists of the S−O_a symmetric and asymmetric stretching modes. Here O_a represents the oxygen atom that is directly bound to the surface.

The assignment of experimentally observed frequencies by computed values is illustrated in Figure 4, parts c−e. Experimentally, SO_2 is the most studied sulfur oxide. Through HREELS[6] and NEXAFS[7] experiments, it was found that SO_2 adsorbed molecularly on clean Pt(111) at temperatures up to 130 K. Three vibrational modes of the chemisorbed molecular SO_2 were detected by HREELS: bending (540 cm^{-1}), symmetric stretching (940 cm^{-1}), and asymmetric stretching (1252 cm^{-1}).[6] A separation of 312 cm^{-1} between the symmetric and asymmetric stretching modes was identified as the unique characteristic of the SO_2 bonding geometry. All of these values closely match our first-principles DFT calculations of SO_2 fcc η^2-S_b,O_a: 524 cm^{-1} (bending), 949 cm^{-1} (symmetric stretching), 1260 cm^{-1} (asymmetric stretching), and 311 cm^{-1} (asymmetric/asymmetric stretching separation). This is demonstrated in Figure 4c by the dotted lines passing through or very close to the crosses. (Refer to Table 6 for the values.)

When the surface heating is continued to 190 K, two new vibrational mode features were observed at 266 and 430 cm^{-1}.[6] Sun et al., however, after comparing them with the known vibrational frequency range of SO_x on other transition metals, did not assign these two new features to any surface species

TABLE 6: Calculated Vibrational Frequencies (cm^{-1}) Corrected by the Correlation in Figure 4a[a]

O fcc	389 (frustrated translation)	389 (frustrated translation)	502 (stretching)		
S fcc	360 (frustrated translation)	362 (frustrated translation)	369 (stretching)		
SO fcc η^1-$S_f(O_f)$	164 (frustrated translation) 1205 (S-O stretching)	166 (frustrated translation)	279 (molecular stretching)	424 (frustrated rotation)	426 (frustrated rotation)
SO fcc η^2-S_b,O_a	146 (frustrated translation) 1012 (S-O stretching)	223 (frustrated translation)	302 (frustrated rotation)	314 (frustrated rotation)	557 (S-Pt stretching)
SO_2 fcc η^2-S_b,O_a	140 (frustrated translation) 324 (out-of-plane deforming)	165 (frustrated translation) 524 (bending)	241 (frustrated rotation) 949 (symmetric stretching)	274 (frustrated rotation) 1260 (asymmetric stretching)	282 (molecular stretching)
SO_2 fcc η^2-S_b,O_a (with metal)	149 (frustrated translation) 328 (out-of-plane deforming)	168 (frustrated translation) 524 (bending)	244 (frustrated rotation) 949 (symmetric stretching)	276 (frustrated rotation) 1260 (asymmetric stretching)	303 (molecular stretching)
SO_2 hcp η^2-S_b,O_a	145 (frustrated translation) 399 (out-of-plane deforming)	179 (frustrated translation) 516 (bending)	231 (frustrated rotation) 992 (symmetric stretching)	254 (frustrated rotation) 1263 (asymmetric stretching)	313 (molecular stretching)
SO_2 fcc η^3-S_a,O_a,O_a	161 (frustrated rotation + frustrated translation) 429 (out-of-plane deforming)	241 (frustrated translation) 495 (bending)	261 (frustrated rotation + frustrated translation) 884 (symmetric stretching)	284 (molecular stretching) 957 (asymmetric stretching)	322 (frustrated rotation + frustrated translation)
SO_3 fcc η^3-S_a,O_a,O_a	137 (O_a-S-O_a frustrated rotation + O_a-S-O_a frustrated translation + S-O* frustrated rotation) 331 (O_a-S-O_a frustrated rotation + S-O* frustrated rotation + O_a-S-O_a frustrated translation) 881 (O_a-S-O_a asymmetric stretching)	176 (frustrated translation + S-O* frustrated rotation) 450 (O_a-S-O_a bending + S-O* frustrated translation) 1285 (S-O* stretching)	198 (S-O* frustrated translation + O_a-S-O_a frustrated translation + O_a-S-O_a frustrated rotation) 514 (O_a-S-O_a frustrated rotation + O_a-S-O_a frustrated translation + S-O* frustrated rotation)	252 (S-O* frustrated rotation + O_b-S-O_b frustrated translation) 613 (O_a-S-O_a out-of-plane deforming + S-O* frustrated rotation)	324 (molecular stretching + S-O* frustrated rotation) 828 (symmetric stretching + S out-of-O_a-O_a-O*- plane deforming)
SO_3 fcc η^3-O_a,O_a,O_a	199 (frustrated rotation)	201 (frustrated translation)	209 (frustrated translation)	345 (molecular stretching)	373 (frustrated rotation)

TABLE 6 (Continued)

	373 (frustrated rotation)	442 (asymmetric stretching) 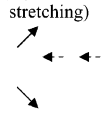	443 (asymmetric stretching) 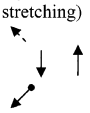	613 (out-of-plane deforming + O_a-O_a-O_a symmetric stretching)	844 (O_a-O_a-O_a symmetric stretching + out-of-plane deforming)
	855 (asymmetric stretching) 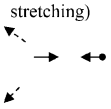	857 (asymmetric stretching) 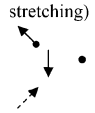			
SO_4 fcc η^3-O_a,O_a,O_a	155 (frustrated rotation)	160 (frustrated transition)	229 (frustrated transition)	244 (S-O* frustrated rotation + S-O_a-O_a-O_a frustrated transition + S-O_a-O_a-O_a frustrated rotation)	245 (S-O_a-O_a-O_a frustrated transition + S-O_a-O_a-O_a frustrated rotation + S-O* frustrated rotation)
	330 (molecular stretching)	440 (S-O_a-O_a-O_a asymmetric stretching) 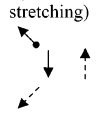	441 (S-O_a-O_a-O_a asymmetric stretching) 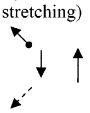	575 (S-O_a-O_a-O_a asymmetric stretching) 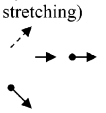 + S-O* frustrated rotation)	575 (S-O_a-O_a-O_a asymmetric stretching) 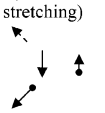 + S-O* frustrated rotation)
	609 (S-O* out-of-O_a-O_a-O_a-plane deforming + O_a-O_a-O_a symmetric stretching)	863 (symmetric stretching)	881 (S-O_a-O_a-O_a asymmetric stretching) 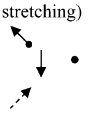	881 (S-O_a-O_a-O_a asymmetric stretching) 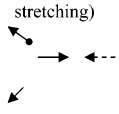	1308 (S-O* stretching)
$(SO_4)_{sr}$ fcc η^3-O_a,O_a,O_a	194 (S-O_a-O_a-O_a frustrated rotation + S-O* frustrated transition)	197 (frustrated transition)	208 (frustrated transition)	259 (S-O* frustrated rotation + S-O_a-O_a-O_a frustrated transition + S-O_a-O_a-O_a frustrated rotation)	272 (S-O_a-O_a-O_a frustrated transition + S-O_a-O_a-O_a frustrated rotation + S-O* frustrated rotation)
	324 (molecular stretching)	464 (S-O_a-O_a-O_a asymmetric stretching 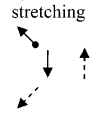 + S-O* frustrated transition)	470 (S-O_a-O_a-O_a asymmetric stretching) 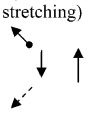	582 (S-O_a-O_a-O_a asymmetric stretching) 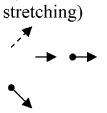 + S-O* frustrated rotation)	585 (S-O_a-O_a-O_a asymmetric stretching) 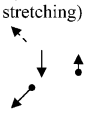 + S-O* frustrated rotation)
	610 (S-O* out-of-O_a-O_a-O_a-plane deforming + O_a-O_a-O_a symmetric stretching)	863 (symmetric stretching)	885 (S-O_a-O_a-O_a asymmetric stretching) 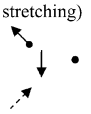	894 (S-O_a-O_a-O_a asymmetric stretching) 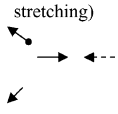	1311 (S-O* stretching)

[a] Note that O_a and O* represent the oxygen atoms that are directly bound and indirectly bound to the metal surface, respectively. When further clarification on the computed normal modes is needed, arrows (with relative scaling length) and dots are used to represent the corresponding vibration directions (with relative scaling strength) and still atoms, respectively. Dotted arrows and dashed arrows are used to represent the additional directions in to and out of the paper, respectively. Arrows and dots at the center represent the sulfur atoms, and the rest of the arrows and dots represent the oxygen atoms.

TABLE 7: Thermodynamics of Elementary Surface Reaction Steps[a]

chemical reactions	reaction index	ΔE(ZPEC) (kJ/mol)	ΔG(298 K, 1 atm) (kJ/mol)	ΔG(600 K, 1 atm) (kJ/mol)
$^1/_2O_2(g) + SO_2(g) \leftrightarrow SO_3(g)$	1	−70.18	−48.39	−23.79
$^1/_2O_2(g) \leftrightarrow O(a)$	2h	−87.14	−60.46	−32.85
$SO_2(g) \leftrightarrow SO_2(a)$	3h	−92.02	−34.05	23.83
$SO_3(g) \leftrightarrow SO_3(a)$	4h	−110.50	−49.64	10.65
$S(a) + O(a) \leftrightarrow SO(a)$	5h	8.93		
$SO(a) + O(a) \leftrightarrow SO_2(a)$	6h	−15.34		
$SO_2(a) + O(a) \leftrightarrow SO_3(a)$	7h	−1.51		
$SO_3(a) + O(a) \leftrightarrow SO_4(a)$	8h	−13.08		
$O_2(g) + S(a) \leftrightarrow SO_2(a)$	9h = 2h + 2h + 5h + 6h	−180.70	−136.00	−91.11
$^1/_2O_2(g) + SO(a) \leftrightarrow SO_2(a)$	10h = 2h + 6h	−102.49	−79.65	−56.25
$^1/_2O_2(g) + SO_2(a) \leftrightarrow SO_3(a)$	11h = 2h + 7h	−88.65	−63.98	−36.98
$O_2(g) + SO_2(a) \leftrightarrow SO_4(a)$	12h = 2h + 2h + 7h + 8h	−188.88	−139.40	−85.08
$SO_2(g) + O(a) \leftrightarrow SO_3(a)$	13h = 3h + 7h	−93.53	−37.57	19.70
$SO_2(g) + SO_2(a) \leftrightarrow SO(a) + SO_3(a)$	14h = 3h + 7h − 6h	−78.19	−18.38	43.11
$SO_2(g) + SO_2(a) \leftrightarrow S(a) + SO_4(a)$	15h = 3h + 7h − 6h + 8h − 5h	−100.20	−37.16	29.86
$2SO(a) \leftrightarrow S(a) + SO_2(a)$	16h = 6h − 5h	−24.27	−23.04	−21.39
$2SO_2(a) \leftrightarrow SO(a) + SO_3(a)$	17h = 7h − 6h	13.83	15.67	19.27
$2SO_2(a) \leftrightarrow S(a) + SO_4(a)$	18h = 7h − 6h + 8h − 5h	−8.18	−3.11	6.03
$2SO_3(a) \leftrightarrow SO_2(a) + SO_4(a)$	19h = 8h − 7h	−11.57	−11.40	−11.13
$SO(a) + SO_2(a) \leftrightarrow S(a) + SO_3(a)$	20h = 7h − 5h	−10.44	−7.38	−2.12
$SO(a) + SO_3(a) \leftrightarrow S(a) + SO_4(a)$	21h = 8h − 5h	−22.01	−18.78	−13.24
$SO(a) + SO_4(a) \leftrightarrow SO_2(a) + SO_3(a)$	22h = 6h − 8h	−2.26	−4.26	−8.15

[a] Note that values in this table correspond to the case of $^1/_4$ ML coverage, which can be regarded as the *high coverage limit*. The third column shows the adsorption energy with zero-point energy corrections at 0 K. A few redundant but important reactions are listed for convenience.

but concluded that the new vibrational features were most likely due to the depletion of some remaining multilayer SO_2.[6] Our DFT calculations indicate two potential matches: (a) SO_2 in the 10 kJ mol^{-1} metastable fcc η^3-S_a,O_a,O_a configuration, with calculated bands at 261 (frustrated rotation and frustrated translation) and 429 cm^{-1} (out-of-plane deforming), and (b) SO in the most stable fcc η^1-$S_f(O_f)$ configuration, with features at 279 (molecular stretching) and 426 cm^{-1} (frustrated rotation), possibly from SO_2 dissociation. The latter of these possible identifications is illustrated in Figure 4d, where the dashed lines pass through the triangles. (Refer to Table 6 for the numerical values.) As we shall discuss in section III, parts E and F, molecularly chemisorbed SO is energetically unstable at high coverages and energetically stable at low coverages with respect to molecularly chemisorbed SO_2. The systems studied via HREELS are likely best modeled in the high coverage limit. Therefore, we conclude that the HREELS features at 266 and 430 cm^{-1} are most likely due to vibrational motions of the flat-lying SO_2 fcc η^3-S_a,O_a,O_a. This also serves as an explanation of the experimental observation of the flat-lying chemisorbed SO_2 in the NEXAFS experiment between 148 and 212 K by Polcik et al.[7] On the other hand, at low coverages, features at 266 and 430 cm^{-1} would be most likely due to the molecularly chemisorbed SO, provided that the dissociation of SO to atomic S and O is kinetically inhibited on Pt(111).

After annealing the surface to 300 K, Sun et al. obtained fuzzy HREELS spectra. These were suggested to be due to highly oxidized sulfur species, such as SO_4.[6] Slightly cleaner spectra at high temperatures were reported three years later by Wilson et al. in their HREELS study of the chemisorption of SO_2 on both the clean and oxygen precovered Pt(111) surfaces.[8] Similar to the previous experimental results and our computational results, they also obtained the three vibrational modes (525, 940, and 1245 cm^{-1}) of molecular SO_2 on clean Pt(111) at low temperature (160 K). But they did not detect any differences other than intensity loss in the spectra when the system was heated to 270 K, contradictory to the HREELS observations by Sun et al.[6] However, when molecular SO_2 was dosed to an oxygen precovered Pt(111) surface at 160 K, three other vibrational modes centered at 610, 855, and 1252 cm^{-1} were obtained by Wilson et al.[8] Upon annealing, the mode centered at 1252 cm^{-1} broadens to yield two new features centered at 1150 and 1300 cm^{-1}, respectively. This change was interpreted by Wilson et al.[8] to signify formation of surface SO_4. Three vibrational modes are consistent with our computed values of a) 613 (O_a−S_a−O_a out of plane deforming and S−O* frustrated rotation), 828 (symmetric stretching and S out-of- O_a,O_a,O_a*-plane deforming), and 1285 cm^{-1} (S−O* stretching) for SO_3 fcc η^3-S_a,O_a,O_a, and (b) 609 (S out-of-O_a,O_a,O_a*-plane deforming and O_a,O_a,O_a symmetric stretching), 863 (symmetric stretching), and 1308 cm^{-1} (S−O* stretching) for SO_4 fcc η^3-O_a,O_a,O_a. These are demonstrated in Figure 4e by the solid lines passing through or near the stars/filled circles. (Refer to Table 6 for the numerical values.) We did not, however, obtain any modes centered around ∼1150 cm^{-1}, which in fact falls into one of the gaps of our computed vibrational bands. As we shall discuss in sections E−G, molecularly chemisorbed SO_4 is more stable than SO_3 at all coverages. Therefore, we conclude that at chemical equilibrium the HREELS features at 610, 855, and 1300 cm^{-1} are most likely due to chemisorbed SO_4.

E. Reaction Thermodynamics in the High Coverage Limit. To understand the chemistry of sulfur oxides on Pt(111), it is useful to compute the thermodynamics of chemisorption and surface chemical reactions as a function of coverage. A general treatment of surface thermodynamics requires a detailed knowledge of the interactions between all potential surface species,[30,31] which is a significant undertaking for a system as complicated as the sulfur oxides on Pt. Steps toward that goal are currently in progress in our laboratory. Here we consider an approximate treatment of the energetics in three coverage extremes, namely, a high sulfur oxide coverage limit based on the $^1/_4$ ML coverage energies in section III.E, a low sulfur oxide coverage limit based on the extrapolated zero coverage adsorption energies in section III.F, and a high O coverage limit that starts from the p(2×2)−O-saturated surface in section III.G. Thermodynamic free energies at low temperatures (0 K) and intermediate temperatures (298 and 600 K) of all the surface reactions up to bimolecular reactions are listed in Table 7 (reaction 1 and 2h−22h) and Table 8 (reaction 1 and 2l−22l) for the high and low coverage limits, respectively. At low temperatures, the zero-

TABLE 8: Thermodynamics of Elementary Surface Reaction Steps[a]

chemical reactions	reaction index	ΔE_∞(ZPEC) (kJ/mol)	ΔG_∞(298 K, 1 atm) (kJ/mol)	ΔG_∞(600 K, 1 atm) (kJ/mol)
$^1/_2O_2(g) + SO_2(g) \leftrightarrow SO_3(g)$	1	−70.18	−48.39	−23.79
$^1/_2O_2(g) \leftrightarrow O(a)$	2l	−105.96	−79.27	−51.66
$SO_2(g) \leftrightarrow SO_2(a)$	3l	−123.96	−65.99	−8.11
$SO_3(g) \leftrightarrow SO_3(a)$	4l	−147.93	−87.07	−26.78
$S(a) + O(a) \leftrightarrow SO(a)$	5l	29.31		
$SO(a) + O(a) \leftrightarrow SO_2(a)$	6l	9.74		
$SO_2(a) + O(a) \leftrightarrow SO_3(a)$	7l	11.82		
$SO_3(a) + O(a) \leftrightarrow SO_4(a)$	8l	−14.97		
$O_2(g) + S(a) \leftrightarrow SO_2(a)$	9l = 2l + 2l + 5l + 6l	−172.87	−128.40	−83.28
$^1/_2O_2(g) + SO(a) \leftrightarrow SO_2(a)$	10l = 2l + 6l	−96.22	−73.38	−49.99
$^1/_2O_2(g) + SO_2(a) \leftrightarrow SO_3(a)$	11l = 2l + 7l	−94.14	−69.47	−42.46
$O_2(g) + SO_2(a) \leftrightarrow SO_4(a)$	12l = 2l + 2l + 7l + 8l	−215.07	−165.60	−111.03
$SO_2(g) + O(a) \leftrightarrow SO_3(a)$	13l = 3l + 7l	−112.14	−56.18	1.09
$SO_2(g) + SO_2(a) \leftrightarrow SO(a) + SO_3(a)$	14l = 3l + 7l − 6l	−121.88	−62.08	−0.59
$SO_2(g) + SO_2(a) \leftrightarrow S(a) + SO_4(a)$	15l = 3l + 7l − 6l + 8l − 5l	−166.16	−103.10	−36.10
$2SO(a) \leftrightarrow S(a) + SO_2(a)$	16l = 6l − 5l	−19.57	−18.34	−16.69
$2SO_2(a) \leftrightarrow SO(a) + SO_3(a)$	17l = 7l − 6l	2.08	3.91	7.52
$2SO_2(a) \leftrightarrow S(a) + SO_4(a)$	18l = 7l − 6l + 8l − 5l	−42.20	−37.13	−27.99
$2SO_3(a) \leftrightarrow SO_2(a) + SO_4(a)$	19l = 8l − 7l	−26.79	−26.62	−26.34
$SO(a) + SO_2(a) \leftrightarrow S(a) + SO_3(a)$	20l = 7l − 5l	−17.49	−14.43	−9.17
$SO(a) + SO_3(a) \leftrightarrow S(a) + SO_4(a)$	21l = 8l − 5l	−44.23	−41.05	−35.51
$SO(a) + SO_4(a) \leftrightarrow SO_2(a) + SO_3(a)$	22l = 6l − 8l	24.71	22.71	18.82

[a] Note that values in this table correspond to the *low coverage limit*, while the phonon data are taken from the equilibrium surface geometry at the $^1/_4$ ML coverage. The third column shows the adsorption energy with zero-point energy corrections at 0 K. A few redundant but important reactions are listed for convenience.

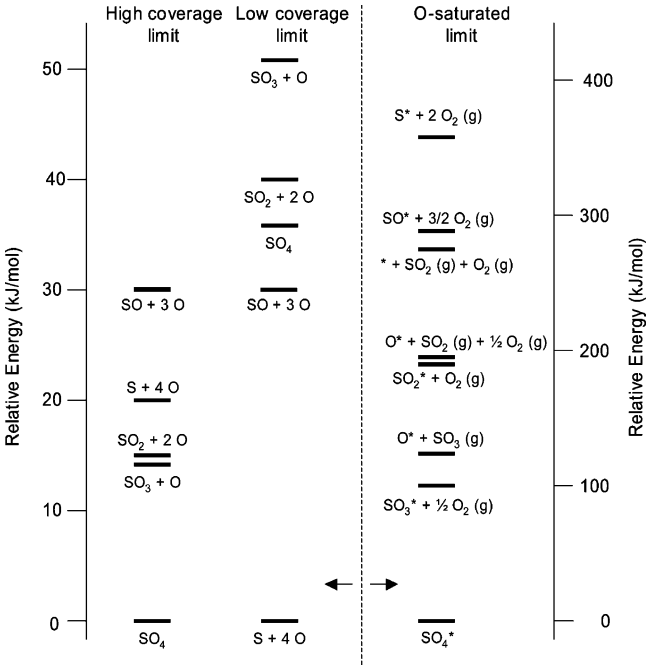

Figure 5. Relative zero-point corrected energies of sulfur oxide adsorbates on Pt(111) in three limits of coverage. In the high (section III.E) and low (section III.F) coverage limits all species are surface bound. In the O-saturated limit (section III.G) adsorption sites on the p(2×2)−O lattice species are denoted explicitly with an asterisk. Note that different energy scales apply to the left two and the right columns.

point energy corrections are computed from the vibrational spectra calculated in section III.D and listed in the third columns of both Tables 7 and 8. The relative stability of different sulfur oxide species at low temperatures is illustrated schematically in Figure 5. The finite temperature contributions are treated differently for different reactants and products, reflecting the importance of different types of entropic effects. For reactions that generate or consume gaseous species, we assume that changes in reaction entropies are dominated by the gas-phase species, whose translational, rotational, and vibrational contributions to gas-phase are obtained from standard ideal gas expressions.[19] We further assume that there are no changes in reaction entropies of either adsorbate configurations or substrate binding sites with temperatures, and therefore the entropy of adsorbates can be adequately modeled by the statistical mechanics of normal modes, using the vibrational spectra calculated in section III.D. However, the assumption of having negligible changes in the entropies of surface binding sites (using only vibrational modes to compute the entropy differences) may be especially inaccurate for dissociation reactions (reaction 5h−8h and reaction 5l−8l), and thus, the analyses of these reactions at intermediate temperatures will not be treated in this work. All other reactions have the same number of adsorbates as reactants and as products, and thus, we assume that errors in our assumption of the form of the entropy calculations cancel. While idealized, these representations provide useful references for deriving qualitative insights into sulfur oxide surface chemistry at extremes of coverage.

In the high coverage limit, the $^1/_4$ ML adsorption energies are assumed to adequately incorporate the lateral interactions experienced by adsorbates on a mixed or partially covered surface. For example, the dissociation of chemisorbed SO to atomic S and O can be written explicitly in this limit as

$$\text{Pt(111)}-\text{p(2}\times\text{2)}-\text{SO(a)} + \text{Pt(111)} \rightarrow \text{Pt(111)}-\text{p(2}\times\text{2)}-\text{S(a)} + \text{Pt(111)}-\text{p(2}\times\text{2)}-\text{O(a)}$$

and can be considered conceptually to occur between islands of S, O, and SO adsorbates, each at $^1/_4$ ML coverage, and patches of bare surface, with the interfaces between these regions assumed to have negligible impact on the thermodynamics. From Figure 5, the surface species decrease in stability in the order of $SO_4 > SO_3 + O > SO_2 + 2O > S + 4O > SO + 3O$. Thus, SO_4, SO_3, and SO_2 are all stable to dissociation in the high coverage limit, and in the presence of surface O, thermodynamics tends toward the production of the most highly oxidized species possible. The stability of SO_2 toward dissociation to SO or atomic S at low temperatures is consistent with

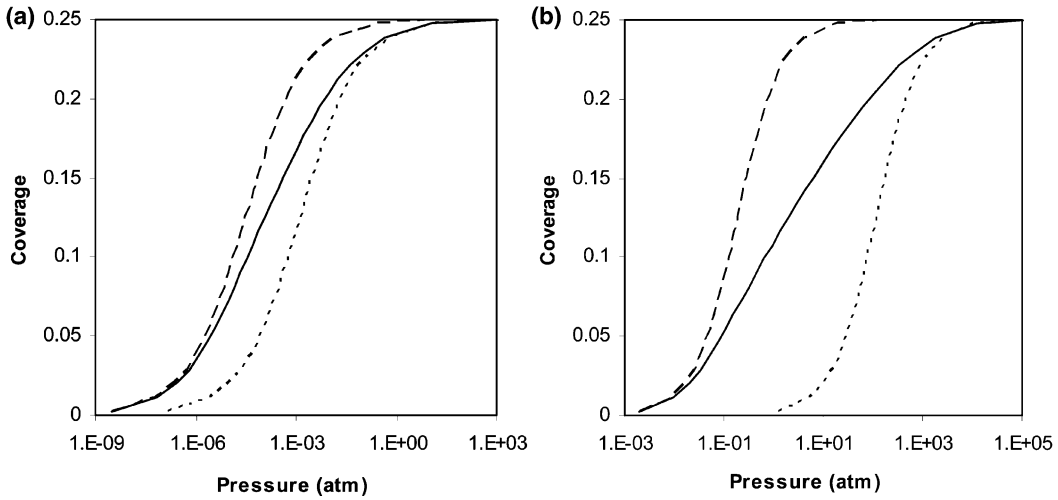

Figure 6. Isotherms of (a) dissociatively chemisorbed O_2 and (b) molecularly chemisorbed SO_2 on Pt(111) at 600 K including the corrections made via the dipole rule of the binding energies (solid lines), the lower bound of Langmuir isotherms with the binding free energy at the zero coverage limit (dashed lines), and the upper bound of Langmuir isotherms with the binding free energy at $^1/_4$ ML coverage (dotted lines).

experimental observations.[6,8] Interestingly, SO is predicted to be unstable to dissociation to the atoms even at high coverages.

Disproportionation of chemisorbed SO_2 to SO and SO_3 is unfavorable by 14 kJ/mol (reaction 17h), but disproportionation to S and SO_4, is favored by 8 kJ/mol (reaction 18h). That experiments have not detected any surface species other than SO_2 at low temperature suggests that this disproportionation (reaction 18h) is slow at experimental temperatures. Similarly, both SO and SO_3 are thermodynamically unstable with respect to disproportionation to S and SO_2 (reaction 16h) and to SO_2 and SO_4 (reaction 19h), respectively.

F. Reaction Thermodynamics in the Low Coverage Limit. The energetics of adsorption in the low coverage limit can be obtained from the extrapolated adsorption energies of Figure 2. As shown in the middle column of Figure 5 (refer to Table 8 for detailed values), the zero-point-corrected relative energies of surface sulfur species in this limit decrease in the order of S + 4O > SO + 3O > SO_4 > SO_2 + 2O > SO_3 + O, differing significantly from the trend found in the high coverage limit. In the low coverage limit, all of the sulfur oxides are energetically unstable to dissociation to the elements, in contrast with the stability of all the sulfur oxides save SO to complete dissociation at high coverage. In the absence of destabilizing lateral interactions, Pt−S and Pt−O bonding more than compensates for the loss of S−O bonding on dissociation. Surface-bound SO_4 does evidence some greater intrinsic stability than SO_3 and SO_2, as dissociation of SO_4 to SO_3 and O or to SO_2 and 2O are both energetically uphill. The large adsorption energy of atomic O and the absence of lateral repulsions in this limit eventually overwhelm the internal SO_x bonding, and further dissociation to SO and 3O or S and 4O is energetically driven. Thus, the existence of sulfur oxides as isolated molecular entities on Pt(111) is a consequence of some combination of lateral interaction and kinetic effects, and is not an inherent thermodynamic property of the adsorbates. This conclusion is similar to that recently reported for the oxidation of NO to NO_2 on Pt(111) based on DFT calculations, in which it was found that NO_2 formation was unfavored at low coverages and favored at higher coverages.[31]

Comparing the data in Table 8 for the low coverage limit with the data in Table 7 for the high coverage limit, one finds that the Gibbs free energies at 600 K of a few important surface chemical reactions change signs, reflecting the strong coverage dependence of these reactions. For example, in the absence of destabilizing lateral interactions, chemisorption of SO_2 and SO_3 at 600 K (reaction 3l and reaction 4l, respectively) is much more favored than at high coverage. This implies that, even though one may detect the desorption of a significant portion of sulfur oxides from Pt(111) at 600 K (reactions 3h and 4h),[6,8] higher temperatures are needed for the complete desorption of residual surface sulfur oxides. Moreover, at low coverages, all of the Eley−Rideal reactions (involving either gas-phase O_2 or gas-phase SO_2, reactions 9l−15l) have negative $\Delta G°$, except for the oxidation reaction between gas-phase SO_2 and chemisorbed O that forms chemisorbed SO_3 (reaction 13l).

Experimentally, upon chemisorption of pure SO_2, Wilson et al. found no changes other than the loss of intensity in the HREELS signature for SO_2 upon annealing from 160 to 350 K, but Sun et al. reported the formation of both SO_4 and SO upon annealing from 190 to 300 K.[6,8] These contradictory observations from HREELS experiments concerning whether the chemisorbed SO_2 dissociates or not at temperatures between 190 and 300 K reflects the overriding importance of coverage and kinetic effects in controlling the surface composition of the surface species.[32]

One of the most striking observations from our first-principles computations is that, without exception, all reactions that produce chemisorbed SO_4 are favorable in the low coverage limit. This conclusion is similar in the high coverage case. These observations imply that SO_4 is a very stable surface species on Pt(111), consistent with experimental evidence.[5,8,33]

G. Reaction Thermodynamics in the High Oxygen Coverage Limit. An important practical limit to consider is that of the interaction of SO_x species with an oxygen-saturated surface. Such a limit is relevant, for instance, to the oxidation of SO_x that occurs on Pt catalysts in the presence of excess O_2.[5,8] As shown in Table 7, the oxidation of SO_2 to SO_3 in the gas phase is favored ($\Delta G° < 0$) at standard conditions from 0 to greater than 600 K (refer to reaction 1), consistent with the known thermodynamics that show oxidation to be favorable up to 1100 K.[34] That oxidation does not occur in the absence of a transition metal oxidation catalyst at 600 K indicates that the oxidation process is kinetically limited in the gas phase. This temperature is at the low-end of operation of typical automotive catalysts.[35]

In this section, we consider a Pt(111) surface covered with an overlayer of O atoms, Pt(111)−p(2×2)−O, the structure that would be expected to exist in the presence of a significant concentration of gaseous O_2. We assume that SO_x adsorbates

can exist only at the sites of the p(2×2)−O lattice, i.e., we ignore adsorption and reaction that might occur at interstitial fcc or other sites. The SO_x adsorption energy at a vacant site in the p(2×2)−O lattice is approximated by the high coverage SO_x adsorption energy described in section III.E. This latter approximation is equivalent to assuming that the SO_x−O lateral interactions on the p(2×2) surface are the same as the SO_x−SO_x lateral interactions at the same coverage. As an example, within this model, SO_2 chemisorbs either directly onto an O surface sites (an Eley−Rideal reaction) or by displacement of surface O to the gas phase. The first reaction can be written

$$\mathrm{Pt^*{-}O(a)} + \mathrm{SO_2(g)} \leftrightarrow \mathrm{Pt^*{-}SO_3(a)}$$

where "Pt*" represents a particular site on the Pt(111)−p(2×2) lattice, and from Table 7 has an energy of −94 kJ/mol in this model. The second, O displacement, reaction can be written

$$\mathrm{Pt^*{-}O(a)} + \mathrm{SO_2(g)} \leftrightarrow \mathrm{Pt^*{-}SO_2(a)} + {}^1/_2\mathrm{O_2(g)}$$

and its energy is calculated as a combination of the O desorption energy (87 kJ/mol) and SO_2 adsorption energy (−92 kJ/mol), for a net energy of −5 kJ/mol. Similar calculations yield the relative energy ordering shown on the right side of Figure 5.

The relative energetics in this limit are different from those considered above in the high and low coverage limits. As in the high coverage limit, more highly oxidized SO_x species are progressively favored on the Pt(111) surface, but the presence of a reservoir of oxygen greatly increases the driving force toward oxidation. In this limit the energetic ordering becomes $SO_4 > SO_3 > SO_2 > SO > S$, where the differences between each are on the order of 100 kJ/mol. The energetically preferred SO_x product in the presence of excess O_2 is thus SO_4, consistent with experimental observation of SO_4 at low temperatures on the oxygen precovered Pt(111) surface.[8]

H. Isotherms. Combining the computed Gibbs free energies and the coverage dipole rule, one obtains (non-Langmuirian) isotherms, having coverage θ dependent binding free energies:

$$G(\theta) = E[r(\theta)] - TS + PV = E_\infty - \mu_\infty{}^2\left(\frac{\sqrt{\theta}}{r_0}\right)^3 - TS + PV$$

where E_∞, μ_∞, and r_0 are the zero-coverage binding energy, the zero-coverage permanent dipole, and the physical separation of the two nearest adsorbates at the saturated coverage. The coverage, θ, is defined with respect to a saturated coverage of $^1/_4$ ML, or one adsorbate per four Pt surface atoms. Thus, in this equation, $\sqrt{\theta}/r_0$ is effectively the distance between dipoles and is used to compute the dipole−dipole repulsion correction to the zero-coverage binding energy, E_∞. *S* and *PV* are computed as described at the end of section II, namely, via the ideal gas approximation, the harmonic approximation, and by ignoring configurational entropy. We also assume that all of the surface *PV* terms are equal.

The isotherm of the dissociatively chemisorbed O_2 is plotted in Figure 5a, and the isotherm of molecularly chemisorbed SO_2 is plotted in Figure 5b, both of which were computed at a temperature of 600 K. At this temperature, one would expect to have ∼20% of the saturated coverage of O for an oxygen partial pressure of 0.2 atm and < 1% of the saturated coverage of SO_2 for a SO_2 partial pressure of 100 ppm. (Note that both saturated coverages are $^1/_4$ ML.) The isotherms also emphasize the importance of including accurately the adsorbate−adsorbate interactions.

IV. Conclusions

We report here the first systematic study using accurate supercell-based DFT calculations of the stable and metastable adsorption states of the entire series of sulfur oxides, including S, O, SO, SO_2, SO_3, and SO_4, on a Pt(111) surface. The sulfur atoms of the most energetically stable SO_x ($x = 1$, 2, 3, and 4) surface species exhibit a general tetrahedral binding preference to x oxygen atoms and $4 - x$ surface Pt atoms. By examination of adsorbates at various levels of coverage and using the previously reported[14] dipole interaction rule, adsorption energies in the limits of high coverage and low coverage are obtained. In the limit of low coverage, all the SO_x species are energetically unstable with respect to dissociation to adsorbed atomic S and O. Experimental observations of adsorbed SO_x on Pt(111) at low coverage is thus a consequence of the slow rate of dissociation. Because of lateral interactions among adsorbate species, in the high sulfur oxide coverage limit, reaction energetics are quite different, and the sulfur oxides tend to be energetically stable to dissociation. High coverages can also lead to surface reconstructions. Various disproportionation reactions are, however, energetically possible, even at high coverages, a result that is consistent with the experimentally observed coverage-dependent disproportionation of SO_2 on Pt(111).

In the lean-NO_x automotive exhaust after-treatment system that motivated this work, the surface of a Pt catalyst is expected to be oxygen-covered, and two models are considered here for sulfur oxide surface chemistry under these conditions. Both models lead to the same conclusions: the dominant sulfur oxide species becomes SO_4, which is predicted to be highly stable on the O-covered Pt surface. SO_4 is not stable in the gas phase, and thermal desorption from this species is expected to release SO_3. SO_4 is thus a likely intermediate or spectator in the Pt-catalyzed oxidation of SO_2 to SO_3.

Acknowledgment. The authors would like to thank S. T. Ceyer (MIT) and A. Bogicevic, K. C. Hass, and C. Wolverton (Ford) for thoughtful discussions. This work was supported by Ford Motor Co. and the National Science Foundation, under Grant No. CTS-9984301.

References and Notes

(1) Rodriguez, J. A.; Hrbek, J. *Acc. Chem. Res.* **1999**, *32*, 719.
(2) Haase, J. *J. Phys. Condens. Matter* **1997**, *9*, 3647.
(3) Lin, X.; Trout, B. L. Chemistry of Sulfur Oxides on Transition Metal Surfaces. In *Interfacial Applications in Environmental Engineering*; Keane, M., Ed.; Marcel Dekker: New York, 2003; Vol. 108; p 55.
(4) Astegger, S.; Bechtold, E. *Surf. Sci.* **1982**, *122*, 491.
(5) Wilson, K.; Hardacre, C.; Lambert, R. M. *J. Phys. Chem.* **1995**, *99*, 13755.
(6) Sun, Y. M.; Sloan, D.; Alberas, D. J.; Kovar, M.; Sun, Z. J.; White, J. M. *Surf. Sci.* **1994**, *319*, 34.
(7) Polcik, M.; Wilde, L.; Haase, J.; Brena, B.; Comelli, G.; Paolucci, G. *Surf. Sci.* **1997**, *381*, L568.
(8) Wilson, K.; Hardacre, C.; Baddeley, C. J.; Ludecke, J.; Woodfuff, D. P.; Lambert, R. M. *Surf. Sci.* **1997**, *372*, 279.
(9) http://www.fysik.dtu.dk/CAMP/dacapo.html.
(10) Vanderbilt, D. *Phys. Rev. B* **1990**, *41*, 7892.
(11) Laasonen, K.; Pasquarello, A.; Car, R.; Lee, C.; Vanderbilt, D. *Phys. Rev. B* **1993**, *47*, 10142.
(12) Lin, X.; Ramer, N. J.; Rappe, A. M.; Hass, K. C.; Schneider, W. F.; Trout, B. L. *J. Phys. Chem. B* **2001**, *105*, 7739.
(13) Perdew, J. P.; Chevary, J. A.; Vosko, S. H.; Jackson, K. A.; Pederson, M. R.; Singh, D. J.; Fiolhais, C. *Phys. Rev. B* **1992**, *46*, 6671.
(14) Lin, X.; Hass, K. C.; Schneider, W. F.; Trout, B. L. *J. Phys. Chem. B* **2002**, *106*, 12575.
(15) Kresse, G.; Furthmuller, J. *Comput. Mater. Sci.* **1996**, *6*, 15.
(16) Wagner, F.; Laloyaux, T.; Scheffler, M. *Phys. Rev. B* **1998**, *57*, 2102.
(17) Bogicevic, A.; Strömquist, J.; Lundqvist, B. I. *Phys. Rev. B* **1998**, *57*, R4289.

(18) Goldstein, H.; Poole, C.; Safko, J. *Classical Mechanics*, 3rd ed.; Addison-Wesley: San Francisco, CA, 2002.

(19) McQuarrie, D. A. *Statitistical Mechanics*; Harper Collins Publishers: New York, 1976.

(20) Starke, U.; Materer, N.; Barbieri, A.; Döll, R.; Heinz, K.; Van Hove, M. A.; Somorjai, G. A. *Surf. Sci.* **1993**, *287/288*, 432.

(21) Parker, D. H.; E.; B. M.; Koel, B. E. *Surf. Sci.* **1989**, *217*, 489.

(22) Billy, J.; Abon, M. *Surf. Sci.* **1984**, *146*, L525.

(23) Yang, Z.; Wu, R.; Rodriguez, J. A. *Phys. Rev. B* **2002**, *65*, 155409.

(24) Rodriguez, J. A.; Ricart, J. M.; Clotet, A.; Illas, F. *J. Chem. Phys.* **2001**, *115*, 454.

(25) Schneider, W. F.; Li, J.; Hass, K. C. *J. Phys. Chem. B* **2001**, *105*, 6972.

(26) Jackson, G. J.; Driver, S. M.; Woodruff, D. P.; Abrams, N.; Jones, R. G.; Butterfield, M. T.; Crapper, M. D.; Cowie, B. C. C.; Formoso, V. *Surf. Sci.* **2000**, *459*, 231.

(27) Polcik, M.; Wilde, L.; Haase, J. *Phys. Rev. B* **1998**, *57*, 1868.

(28) Broekmann, P.; Wilms, M.; Spaenig, A.; Wandelt, K. *Prog. Surf. Sci.* **2001**, *67*, 59.

(29) Driver, S. M.; Woodfuff, D. P. *Surf. Sci.* **2001**, *479*, 1.

(30) Stampfl, C.; Kreuzer, H. J.; Payne, S. H.; Pfnür, H.; Scheffler, M. *Phys. Rev. Lett.* **1999**, *83*, 2993.

(31) Ovesson, S.; Lundqvist, B. I.; Schneider, W. F.; Bogicevic, A. *Phys. Rev. Lett.* **2003**, submitted for publication.

(32) Rodriguez, J. A.; Jirsak, T.; Chaturvedi, S.; Herbek, J. *J. Am. Chem. Soc.* **1998**, *120*, 11149.

(33) Lee, A. F.; Wilson, K.; Lambert, R. M.; Hubbard, C. P.; Hurley, R. G.; McCabe, R. W.; Gandhi, H. S. *J. Catal.* **1999**, *184*, 491.

(34) Chase, M. W., Jr. *NIST-JANAF Thermochemical Tables*, 4th ed.; ACS and AIP for NIST: Washington, DC, 1999.

(35) Taylor, K. C. Automobile Catalytic Converters. In *Catalysis Science and Technology*; Anderson, J. R., Boudart, M., Eds.; Springer-Verlag: Berlin, 1984; Vol. 5; p 119.

(36) http://webbook.nist.gov.

(37) Lehwald, S.; Ibach, H.; Steininger, H. *Surf. Sci.* **1982**, *117*, 342.